Inorg. Chem. **2009**, *48*, 663−670

Para-Hydrogen Induced Polarization without Incorporation of *Para*-Hydrogen into the Analyte

Kevin D. Atkinson,[†] Michael J. Cowley,[†] Simon B. Duckett,*[,†] Paul I. P. Elliott,[‡] Gary G. R. Green,[§] Joaquín López-Serrano,[†] Iman G. Khazal,[†] and Adrian C. Whitwood[†]

Department of Chemistry, University of York, Heslington, York YO10 5DD, U.K., and York Neuroimaging Centre, The Biocentre, York Science Park, Innovation Way, Heslington, York YO10 5DD, U.K.

Received October 20, 2008

The cationic iridium complexes $[Ir(COD)(PR_3)_2]BF_4$ (**1a-c**) (a, R = Ph; b, R = *p*-tolyl; c, R = *p*-C_6H_4−OMe) react with parahydrogen in the presence of pyridine to give *trans*, *cis*, *cis*-$[Ir(PR_3)_2(py)_2(H)_2]^+$ (**2a-c**) and small amounts of *fac*, *cis*-$[Ir(PR_3)(py)_3(H)_2]^+$ (**3a-c**), each of which exhibit polarized hydride resonances due to the magnetic inequivalence associated with the resultant AA"XX" spin system when ^{15}N-labeled pyridine is employed. The pyridine ligands in **2** are labile, exchanging slowly into free pyridine with a rate constant of 0.4 s^{-1} for **2a** at 335 K in a dissociative process where $\Delta H^{\ddagger} = 134 \pm 1$ kJ mol^{-1} and $\Delta S^{\ddagger} = 151 \pm 5$ J mol^{-1} K^{-1}. Pyridine ligand exchange in **2** proves to be slower than that determined for **3**. Parahydrogen induced polarization (PHIP) based on the hydride ligands of **2** and **3** is transferred efficiently to the ^{15}N nuclei of the bound pyridine ligand by suitable insensitive-nuclei-enhanced-by-polarization-transfer (INEPT) based procedures. Related methods are then used to facilitate the sensitization of the free pyridine ^{15}N signal by a factor of 120-fold through ligand exchange even though this substrate does not contain parahydrogen. This therefore corresponds to the successful polarization of an analyte by parahydrogen induced polarization methods without the need for the actual chemical incorporation of any parahydrogen derived nuclei into it.

Introduction

Over the past two decades parahydrogen enhanced NMR spectroscopy[1] has proved to be a powerful tool for the study of reaction mechanisms involving H_2.[2−4] During these studies several reaction intermediates have been detected and their kinetic fate monitored.[5−10] Low concentration products present in H_2 addition equilibria have also been detected using this approach.[11,12] This method, relies on the fact that parahydrogen (p-H_2), the nuclear spin isomer of dihydrogen with the spin configuration $\alpha\beta$-$\beta\alpha$, can be easily isolated. Reactions with p-H_2 then lead to products that are initially formed with a nuclear spin distribution that at best reflects that of the original dihydrogen molecule. In this way non-Boltzmann spin distributions can be produced in such reaction products which lead to significant signal enhancements in their ^1H NMR spectra. It is for this reason that

* To whom correspondence should be addressed. E-mail: sbd3@york.ac.uk.
† University of York.
‡ Present Address: Department of Chemical & Biological Sciences, University of Huddersfield, Queensgate, Huddersfield HD1 3DH, U.K.
§ York Neuroimaging Centre.

(1) Bowers, C. R.; Weitekamp, D. P. *J. Am. Chem. Soc.* **1987**, *109*, 5541–5542.
(2) Duckett, S. B.; Sleigh, C. J. *Prog. Nucl. Magn. Reson. Spectrosc.* **1999**, *34*, 71–93.
(3) Natterer, J.; Bargon, J. *Nucl. Magn. Reson. Spectrosc.* **1997**, *31*, 293–315.
(4) Eisenberg, R.; Eisenschmid, T. C.; Chinn, M. S.; Kirss, R. U. *A. Chem. Ser.* **1992**, 47–74.
(5) Blazina, D.; Duckett, S. B.; Dyson, P. J.; Lohman, J. A. B. *Angew. Chem., Int. Ed. Engl.* **2001**, *40*, 3874–3876.
(6) Blazina, D.; Duckett, S. B.; Dyson, P. J.; Lohmann, J. A. B. *Chem.—Eur. J.* **2003**, *9*, 1046–1061.
(7) Colebrooke, S. A.; Duckett, S. B.; Lohman, J. A. B.; Eisenberg, R. *Chem.—Eur. J.* **2004**, *10*, 2459–2474.
(8) Duckett, S. B.; Newell, C. L.; Eisenberg, R. *J. Am. Chem. Soc.* **1994**, *116*, 10548–10556.
(9) López-Serrano, J.; Duckett, S. B.; Lledós, A. *J. Am. Chem. Soc.* **2006**, *128*, 9596–9597.
(10) Lopez-Serrano, J.; Duckett, S. B.; Aiken, S.; Lenero, K. Q. A.; Drent, E.; Dunne, J. P.; Konya, D.; Whitwood, A. C. *J. Am. Chem. Soc.* **2007**, *129*, 6513–6527.
(11) Duckett, S. B.; Eisenberg, R. *J. Am. Chem. Soc.* **1993**, *115*, 5292–5293.
(12) Duckett, S. B.; Mawby, R. J.; Partridge, M. G. *Chem. Commun.* **1996**, 383–384.

10.1021/ic8020029 CCC: $40.75
Published on Web 12/15/2008

parahydrogen induced polarization (PHIP) has facilitated the characterization of many species that would otherwise be unobservable by NMR spectroscopy.

The best example of this enhancement is provided by the hydride resonances of the complex $[Ru(dpae)(CO)_2(H)_2]$ (dpae = bis(diphenylarsino)ethane) when it is generated by photolysis of $[Ru(dpae)(CO)_3]$ under a p-H_2 atmosphere.[13,14] The hydride resonances were shown to yield the maximum theoretical signal enhancement of 31,200 at 9.4 T. This situation actually corresponds to the generation of a pure singlet spin state and therefore means that every complex molecule contributes to the detected NMR signal. New insights into reactivity that have resulted from this effect include a more detailed delineation of the role of ruthenium clusters and their fragmentation products in hydrogenation catalysis.[15] Other key species have been detected in cobalt and iridium catalyzed hydroformylation processes through the incorporation of the p-H_2 label into alkyl and acyl ligands within the ligand sphere.[16−18] Similarly, several palladium alkyl and vinyl complexes that play a direct role in alkyne hydrogenation have been detected, characterized, and studied.[10,19] Many of these results have been reviewed.[20,21]

The detection of transition metal dihydride complexes through their hydride resonances is often facilitated because they appear in a normally vacant part of the ^{1}H NMR spectrum, typically between −5 and −25 ppm. The polarization afforded by the PHIP effect therefore allows suitable metal dihydride complexes to act as sensors for substrates in low concentration through the detection of such signals. Here, the chemical shift of the hydride signal is diagnostic of the substrate. We recently reported studies dealing with the detection and dynamics of pyridine coordination derivatives of Wilkinson's complex and its tribenzylphosphine and tricyclohexylphosphine analogues as part of such a study.[22] More significantly, when it was extended to the receptor complex $[Ir(H)_2Cl(PPh_3)_2]$ the binding of purine and adenine substrates demonstrated that their detection at pico-mole levels was possible through such a hydride reporter.[23]

In these and other studies, the hydride-based polarizations have been used to illuminate the coordination sphere of metal complexes by polarization transfer. An early example of such a study dealt with the addition of p-H_2 to $Rh(PMe_3)_4Cl$ and $Rh(PMe_3)_3Cl$, where the dihydride products were used to demonstrate that two-dimensional NMR techniques such as COSY, HSQC, HMQC, and NOESY can be used with p-H_2.[24] Other one-dimensional methods of characterizing hydrogenation products have been developed by Bargon, for example, using a number of modified insensitive-nuclei-enhanced-by-polarization-transfer (INEPT) experiments to obtain ^{13}C spectra of 1,4-diphenylbut-1-en-3-yne, formed via the hydrogenation of 1,4-diphenylbutadiyne.[25]

Here we report on p-H_2 studies dealing with the interaction of cationic dihydride iridium phosphine complexes and pyridine. The complexes employed here are based on the well-known $[Ir(COD)L_2]BF_4$ (COD = 1,3- cyclooctadiene and L = phosphine) system of Crabtree.[26] Groups have prepared and conducted very extensive studies on the reactivity of these and the related complexes $[IrH_2S_2L_2]BF_4$ and $[IrH_2(ol)_2L_2]BF_4$ (S = solvent; ol = olefin) in both hydrogenation and dehydrogenation reactions. Related $[IrH_2S_3L]BF_4$ complexes have also proved to be active in a variety of situations including alkyne dimerization and hydrogenation.[27,28] Our experiments demonstrate that polarization transfer from the hydride ligands to the ^{15}N center of pyridine in $[IrH_2S_2L_2]BF_4$ (S = pyridine) is possible. We also demonstrate that the PHIP effect can be used to enhance the signal strength of the ^{15}N resonance of free pyridine via ligand exchange. This contrasts with the situation found in other, well-reported approaches, to polarization transfer with p-H_2, where the NMR signature of organic materials is enhanced through their formation in a hydrogenation reaction involving an unsaturated version of the substrate.[2−4] This report therefore presents a significant new development in the in situ preparation of hyperpolarized materials.

Results and Discussion

Reactivity of $[Ir(COD)(PPh_3)_2]^+$ Toward H_2 and Pyridine. When H_2 was bubbled through a solution of $[Ir(COD)(PPh_3)_2]BF_4$ (**1a**) in dichloromethane, in the presence of a 2-fold excess pyridine, complex $[Ir(PPh_3)_2(py)_2(H)_2]^+$ (**2a**) was generated. Complex **2a** was isolated, and appropriate NMR based spectroscopic data obtained to confirm its identity on the basis of agreement with previously described data of Rosales et al.[29] The NMR parameters for **2a** can be found in Table 1.

2a was then generated from **1a** in CD_3OD rather than CD_2Cl_2 by adding an 8-fold excess of pyridine and H_2 to this solution at 330 K. When the time course of this reaction was monitored by in situ ^{1}H NMR spectroscopy, the

(13) Anwar, M. S.; Blazina, D.; Carterer, H.; Duckett, S. B.; Halstead, T. K.; Jones, J. A.; Kozak, C. M.; Taylor, R. J. K. *Phys. Rev. Lett.* **2004**, *93*, 040501–040504.
(14) Blazina, D.; Duckett, S. B.; Halstead, T. K.; Kozak, C. M.; Taylor, R. J. K.; Anwar, M. S.; Jones, J. A.; Carteret, H. A. *Magn. Reson. Chem.* **2005**, *43*, 200–208.
(15) Blazina, D.; Duckett, S. B.; Dyson, P. J.; Lohman, J. A. B. *Dalton Trans.* **2004**, 2108–2114.
(16) Godard, C.; Duckett, S. B.; Henry, C.; Polas, S.; Toose, R.; Whitwood, A. C. *Chem. Commun.* **2004**, 1826–1827.
(17) Godard, C.; Duckett, S. B.; Polas, S.; Tooze, R. P.; Whitwood, A. C. *J. Am. Chem. Soc.* **2005**, *127*, 4994–4995.
(18) Permin, A. B.; Eisenberg, R. *J. Am. Chem. Soc.* **2002**, *124*, 12406–12407.
(19) Lopez-Serrano, J.; Lledos, A.; Duckett, S. B. *Organometallics.* **2008**, *27*, 43–52.
(20) Blazina, D.; Duckett, S. B.; Dunne, J. P.; Godard, C. *Dalton Trans.* **2004**, 2601–2609.
(21) Duckett, S. B.; Blazina, D. *Eur. J. Inorg. Chem.* **2003**, *16*, 2901–2912.
(22) Zhou, R. R.; Aguilar, J. A.; Charlton, A.; Duckett, S. B.; Elliott, P. I. P.; Kandiah, R. *Dalton Trans.* **2005**, 3773–3779.
(23) Wood, N. J.; Brannigan, J. A.; Duckett, S. B.; Heath, S. L.; Wagstafft, J. *J. Am. Chem. Soc.* **2007**, *129*, 11012–11013.
(24) Messerle, B. A.; Sleigh, C. J.; Partridge, M. G.; Duckett, S. B. *Dalton Trans.* **1999**, 1429–1435.
(25) Haake, M.; Natterer, J.; Bargon, J. *J. Am. Chem. Soc.* **1996**, *118*, 8688–8691.
(26) Crabtree, R. H.; Mellea, M. F.; Mihelcic, J. M.; Quirk, J. M. *J. Am. Chem. Soc.* **1982**, *104*, 107–113.
(27) Sola, E.; Navarro, J.; Lopez, J. A.; Lahoz, F. J.; Oro, L. A.; Werner, H. *Organometallics.* **1999**, *18*, 3534–3546.
(28) Navarro, J.; Sagi, M.; Sola, E.; Lahoz, F. J.; Dobrinovitch, I. T.; Katho, A.; Joo, F.; Oro, L. A. *Adv. Synth. Catal.* **2003**, *345*, 280–288.
(29) Rosales, M.; Gonzalez, T.; Atencio, R.; Sanchez-Delgado, R. A. *Dalton Trans.* **2004**, 2952–2956.

Table 1. NMR Data for Complexes **2a-c** and **3a-b**[a]

complex		^{1}H/δ	^{31}P/δ	^{13}C/δ	^{15}N/δ[b]
2a	H	−21.64 ($^2J_{PH}$ =17.4 Hz, $^2J_{NH}$ = 20, J_{HH} = −6.4)			
	PPh_3	7.37 (m, J_{HH} = 8.3 Hz, ortho), 7.26 (t, J = 8.3, meta), 7.36 (m, para)	δ 23.0 (s)	131.7 ($^1J_{PC}$ 16 Hz, ipso), 133.7 (o), 128.0 (m), 130.0 (p)	
	Py	8.05 (d, J = 7.0 Hz, o), 6.78 (t, J = 7.0, m), 7.49 (t, J = 7.7, p)		155.8 (o), 125.3 (m), 136.1 (p)	δ −62.2
2b	H	−21.47 (t, $^2J_{PH}$ = 17.6 Hz, $^2J_{NH}$ = 24, $^2J_{HH}$ = −6.5)			
	P(p-Tol)$_3$	7.18 (dd, 7.7 and 6.8 Hz, o), 7.06 (d, 7.7, m), 2.33 (s, CH_3)	δ 22.8 (s)	133.5 (o), 128.6 (m), 140.5 (p), 19.9 (s, CH_3)	
	Py	8.02 (d, J = 5.6 Hz, o), 6.77 (t, J = 7.0, m), 7.50 (t, J = 6.5, p)		155.9 (o), 125.3 (m), 131.7 (p)	δ −62.8
2c	H	−21.73 ($^2J_{PH}$ = 17.1 Hz, $^2J_{NH}$ = 23.3, $^2J_{HH}$ = −6.5)			
	P(p-C_6H_4OMe)$_3$	7.22 (dt, J = 8.0, 5.4 Hz, o), 6.79 (d, J = 8.0 Hz, m), 3.77 (s, OCH_3).	18.2 (s)	127.0 (o), 105.7 (m), 153.4 (p), 115.55 (i), 46.58 (OCH_3)	
	Py	8.05 (d, J = 6 Hz, o), 6.82 (t, J = 7.0, m), 7.54 (t, J = 7.0, p)		148.07 (s, o), 117.6 (s, m), 128.7 (s, p)	δ −62.0
3a	H	−21.8 ($^2J_{PH}$ = 22.7 Hz, $^2J_{NH}$ = 22, J_{HH} = −6.6)			
	PPh_3	7.40 (m, J_{HH} = 8.3 Hz, ortho), 7.23 (t, J = 8.3, meta), 7.33 (m, para)	12.6 (d, $^2J_{PN}$ = 42 Hz)	133.1 (o), 127.8 (m), 129.8 (p)	
	trans-Py	8.48 (d, J = 7.0 Hz, o), 7.15 (t, 7.0, m), 7.73 (t, 7.7, p)		154.5 (s, o), 125.8 (s, m), 136.7 (s, p)	−48.2
	cis-Py	8.90 (d, J = 7.0 Hz, o), 7.40 (t, J = 7.0, m), 7.96 (t, J = 7.7, p)		155.6 (s, o), 124.1 (s, m), 137.0 (s, p)	−64.0
3b	H	−21.75 ($^2J_{PH}$ = 24 Hz, $^2J_{NH}$ = 22)			
	P(p-Tol)$_3$	7.21 (t, J = 8.3 Hz, o), 7.02 (t, J = 8.3,m), 2.32 (s, CH_3)	9.74 (d, $^2J_{PN}$ = 43 Hz)	133.15 (o), 128.14 (m), 19.78 (CH_3)	
	trans-Py	8.43 (d, J = 7.0 Hz, o), 7.13 (t, 7.0, m), 7.78 (t, 7.7, p)		154.65 (o), 125.58 (m), 136.8 (p)	−48.7
	cis-Py	8.97 (d, J = 7.0 Hz, o), 7.39 (t, J = 7.0, m), 7.97 (t, J = 7.7, p)		154.9 (o), 125.83 (m), 137.9 (p)	−64.6 (d, $^2J_{NP}$ = 43 Hz)
3c	H	−21.71 ($^2J_{PH}$ = 23.2 Hz, $^2J_{NH}$ = 22)			
	P(p-C_6H_4OMe)$_3$	7.28 (dd, J = 8.9. 10.9 Hz, o), 6.78 (dd, J = 1.7, 9.0 Hz, m), 3.79 (s, OCH_3)	6.8 (d, $^2J_{PN}$ = 49 Hz)	134.6 (o), 113.1 (m), 160.9 (CO), 123.4 (d, J_{CP} = 66 Hz) 54.4 (CH_3)	
	trans-Py	8.47 (d, J = 4.9 Hz, o), 7.18 (m, 6.6, m), 7.80 (tt, 7.7, 1.6, p)		154.7 (o), 125.65 (m), 136.84 (p)	−48.3
	cis-Py	8.88 (m, J = 6.0 Hz, o), 7.31 (t, J = 7.1, m), 7.94 (tt, J = 7.8,1.6, p)		155.4 (o), 125.9 (m), 137.8 (p)	−64.1 (d, $^2J_{NP}$ = 49 Hz)

[a] All chemical shifts were measured at 295 K in CD_3OD solution. [b] Relative to ^{15}N-pyridine = 0 ppm. *trans*-Py = *trans* to H, *cis*-Py = *cis* to H.

Scheme 1. Reaction of **1** with H_2 in the Presence of Excess Pyridine for Form Complexes **2** and **3** (R= Ph (**a**), *p*-tolyl (**b**) and *p*-C_6H_4−OMe (**c**))

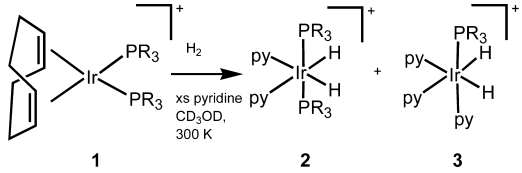

formation of **2a** was indicated by the observation of a dominant hydride signal at δ −21.64 (t, J_{HP} = 17.4 Hz) after a few minutes. The structure of **2a** is indicated in Scheme 1, and it should be noted that the two hydride ligands are chemically equivalent and lie *trans* to pyridine.

The formation of a small amount of a second complex was also indicated in this NMR spectrum, as evidenced by a second hydride signal at δ −21.8. This second hydride signal, due to species **3a**, appears as a simple phosphorus-coupled doublet of 22.7 Hz. The presence of a single phosphorus-hydride splitting suggests that **3a** is a monophosphine complex, and the small value of the J_{PH} coupling indicates that the phosphine ligand is arranged *cis* to the hydride groups. The ^{31}P resonance of the phosphorus center in **3a** was located in an ^{1}H−^{31}P HMQC experiment as a singlet at δ 12.6. When ^{15}N-labeled pyridine was employed in this reaction the corresponding ^{31}P resonance now appears as a nitrogen coupled doublet of 42 Hz. This is indicative of a *trans* phosphine-pyridine ligand arrangement in this monophosphine complex.

More importantly, when this reaction was repeated with ^{15}N-labeled pyridine and *p*-H_2 rather than H_2 the hydride resonances of both **2a** and **3a** appear PHIP enhanced. These signals are illustrated in Figure 1 where the upper trace exhibits both ^{31}P and ^{15}N splittings while the lower trace is ^{31}P decoupled thereby revealing apparent ^{15}N splittings of 20 and 22 Hz, respectively, in addition to the antiphase components, which are separated by −6.4, and −6.6 Hz, respectively. This observation is expected for the hydride resonance of the ^{15}N-labeled isomer of the dihydride complex **2a** since it now belongs to a second order spin system of the type AA"XX". It is the ^{15}N label that makes the hydride ligands magnetically inequivalent and therefore PHIP active. Indeed, when a ^{1}H NMR spectrum is recorded that is ^{15}N decoupled the second order effect is quenched and the PHIP enhancement disappears.

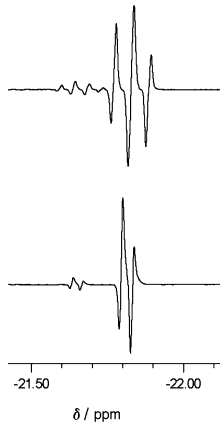

Figure 1. (top) ^{1}H NMR spectrum of the hydride region of a sample containing $[Ir(COD)(PPh_3)_2]^+$ in CD_3OD with ^{15}N-pyridine under *p*-H_2, (bottom) $^1H\{^{31}P\}$ NMR spectrum.

The hydride signals for **3a** show a similar enhancement profile to those of **2a** when the ^{1}H NMR spectrum is recorded with ^{31}P decoupling (Figure 1 (bottom)) and also disappear on ^{15}N decoupling. These observations are therefore indicative of similar ligand arrangements in both **2a** and **3a**. **3a** is therefore confirmed as the dihydride monophosphine *tris*-pyridine complex *fac*, *cis*-$[Ir(PPh_3)(py)_3(H)_2]^+$. It is formed by exchange of one of the phosphine ligands in **2a** with pyridine. The related complex *fac*, *cis*-$[Ir(NCMe)_3(P^iPr_3)(H)_2]^+$ has been described in the literature.[27] One interesting feature that manifests itself in Figure 1 is the relative size of the PHIP enhanced hydride resonances of **3a** and **2a**. In the PHIP enhanced spectra, the hydride signal for **3a** is much larger than that seen for **2a** even though **2a** has the higher real concentration. This effect is reflected in the corresponding $^{31}P\{^1H\}$ NMR spectrum where no signal for **3a** is visible after 128 scans, although that for **2a** is. This situation also agrees with observations when a 9-fold excess of unlabeled pyridine is present since the relative hydride resonance intensities now prove to be 1 to 0.04, respectively. This information suggests therefore that the hydride ligands of complex **3a** exchange with *p*-H_2 at a much greater rate than those of **2a**.

The presence of pyridine within the coordination spheres of complexes **2a** and **3a** was also confirmed by ^{15}N-based NMR spectroscopy. $^1H-^{15}N$ HMQC spectra of the ^{15}N-labeled samples contain correlations between the hydride signals of **2a** and **3a** and resonances in the ^{15}N domain at δ −62.2 and −64.0, respectively. These ^{15}N signals arise from the nitrogen center of the bound pyridine ligands that lie *trans* to hydride.

The NMR parameters for these two complexes are listed in Table 1. The following text describes more fully how complexes **2a** and **3a** were characterized by NMR spectroscopy. First, when a 1D NOE experiment was recorded, the hydride signal at δ −21.64 for **2a** proved to connect with proton signals at δ 8.05 and 7.37, where the latter signal couples strongly to ^{31}P and therefore arises from an *ortho* phenyl proton and the former signal belongs to the *ortho* protons of bound pyridine. When the *ortho* pyridine protons at δ 8.05 are interrogated in a similar way in a 2D experiment, NOE connections to the corresponding *meta* protons at δ 6.78 and the *ortho* phenyl protons of the phosphine at δ 7.37 are visible. The *meta* pyridine protons proved to connect to the corresponding *para* protons which resonate at δ 7.49 in the same experiment. In contrast, the δ 7.37 signal for the phenyl ring connected to a signal at δ 7.26 due to a *meta* proton which connected in turn to a *para* proton signal which appears at δ 7.36. The remaining heteronuclear signals of **2a** were located by HMQC methods, and the corresponding signals for **3a** were attributed by a similar procedure.

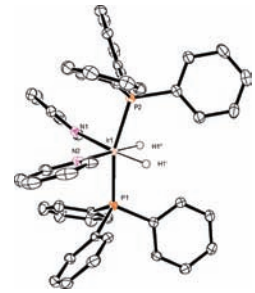

Figure 2. Molecular structure of the cation **2a** (ORTEP). Selected bond distances [Å] and angles (deg): Ir(1)−N(2) 2.177(2), Ir(1)−N(1) 2.196(2), Ir(1)−P(1) 2.2987(6), Ir(1)−P(2) 2.3038(6), N(2)−Ir(1)−N(1) 92.94(8), N(2)−Ir(1)−P(1) 92.89(6), N(1)−Ir(1)−P(1) 100.45(5), N(2)−Ir(1)−P(2) 97.82(6), N(1)−Ir(1)−P(2) 91.61(5), P(1)−Ir(1)−P(2) 163.44(2).

When 2 μL of ^{15}N-labeled pyridine was added to a sample in which **2a** and **3a** had been generated previously using pyridine where the ^{15}N label was present at isotopic abundance, only small levels of PHIP enhancement are observed for the corresponding hydride resonance of **3a** and essentially no enhancement is observed for the corresponding hydride resonance of **2a**. This suggests that the pyridine ligands of both these complexes do not exchange rapidly with free pyridine at 295 K. The enhancement observed for **3a** is, however, compatible with it having a higher rate of exchange than that of **2a**.

X-ray Structure of $[Ir(PPh_3)_2(py)_2(H)_2]^+$ (2a). The crystal structure of **2a** with a BF_4^- counterion is illustrated in Figure 2. Previously Rosales et al. reported the same structure with the PF_6^- counterion.[29] We note that with BF_4^- the P−Ir−P bond angle is 163.44(7)° but with PF_6^- it is 161.00(4)°. Furthermore, the reported Ir−N distances are 2.212(6) and 2.193(7) while here they are 2.177(2) and 2.196(2).

While there are, however, no significant deviations between the Ir−P bond lengths, the N−Ir−N bond angles also vary from 92.94(8)° to 96.3(3)°, respectively. These changes may simply reflect crystal packing effects, but it should be noted that the ability of the precursor complexes as hydrogenation catalysts depends critically on the identity of the anion.[30−32]

Reactions of $[Ir(COD)(P\{p\text{-tolyl}\}_3)_2]^+$ (1b) and $[Ir(COD)(P\{C_6H_4\text{-}4\text{-}OMe\}_3)_2]^+$ (1c) with Pyridine and H_2. To probe the effect of the identity of the phosphine on this reaction, analogues of **2a** and **3a** containing $P\{p\text{-tolyl}\}_3$ and $P\{C_6H_4\text{-}p\text{-}OMe\}_3$ were generated, in situ, using the directly related precursors $[Ir(COD)(P\{p\text{-tolyl}\}_3)_2]^+$, **1b**, and $[Ir(COD)(P\{C_6H_4$-

(30) Crabtree, R. H.; Anton, D. R.; Davis, M. W. *Ann. N.Y. Acad. Sci.* **1983**, *415*, 268–270.
(31) Crabtree, R. H.; Demou, P. C.; Eden, D.; Mihelcic, J. M.; Parnell, C. A.; Quirk, J. M.; Morris, G. E. *J. Am. Chem. Soc.* **1982**, *104*, 6994–7001.
(32) Chodosh, D. F.; Crabtree, R. H.; Felkin, H.; Morris, G. E. *J. Organomet. Chem.* **1978**, *161*, C67–C70.

p-OMe$\}_3)_2]^+$, **1c**, respectively. The NMR data for these species was then collected and assigned in a similar way to that described for **2a**. This information is presented in Table 1.

Reactivity of $[Ir(PPh_3)_2(py)_2(H)_2]^+$ (2a), $[Ir(P\{p\text{-tolyl}\}_3)_2(py)_2(H)_2]^+$ (2b) and $[Ir(P\{C_6H_4\text{-}4\text{-}OMe\}_3)_2(py)_2(H)_2]^+$ (2c). Hydride Ligand Exchange with Dihydrogen. To compare the relative ability of **2** to undergo H_2 exchange, two samples, one containing **1a** and **1b** and the second **1a** and **1c**, were prepared in CD_3OD. They were then exposed to a 15-fold excess of ^{15}N-pyridine and p-H_2 and then examined by ^1H NMR spectroscopy at 295 K. Neither sample showed any PHIP enhancement in the corresponding hydride resonances of **2** or **3** although they were detectable. The samples were then warmed to 330 K and re-examined. At this point, the hydride signals of **2** and **3** were polarized and a series of ^1H, $^1H\{^{31}P\}$, integrateable $^{31}P\{^1H\}$ and 2D HMQC data sets were recorded. These spectra demonstrated that both samples contained signals for the corresponding mixed phosphine dihydride complex. These were $[Ir(PPh_3)(P\{p\text{-tolyl}\}_3)(py)_2(H)_2]^+$ and $[Ir(PPh_3)(P\{p\text{-}C_6H_4\text{-}OMe\}_3)(py)_2(H)_2]^+$ respectively. NMR data for these complexes can be found in the Experimental Section. Key points of interest in these data include the observation of two distinct phosphorus signals for these species which exhibit a strong and mutual PP coupling of around 350 Hz. Furthermore, the dominant hydride signals detected in both samples under PHIP conditions actually corresponded to those of the mono phosphine complexes **3a**, **3b**, and **3c**.

The relative PHIP enhanced hydride signal intensities for **2** obtained from these samples were then determined, and then normalized by dividing them by the relative ^{31}P integral values for these species. The normalized hydride signals intensity ratios determined in this way proved to be 1:1.42:1.9:2.32:3.60 for the species **2a/2b/2c**/$[Ir(PPh_3)(P\{p\text{-tolyl}\}_3)(py)_2(H)_2]^+$/$[Ir(PPh_3)(P\{C_6H_4\text{-}4\text{-}OMe\}_3)(py)_2(H)_2]^+$, respectively. It should be noted that care needs to be employed when interpreting PHIP enhancements since the hydride signal strengths for two dihydride complexes with the same concentration need not be the same because they will reflect both their concentration and their ability to incorporate fresh parahydrogen. This means that the normalized signal intensities for **2** will only reflect the associated rate of introduction of fresh p-H_2 into them. We therefore conclude that the extent of H_2 exchange increases across the series PPh_3 < $P\{p\text{-tolyl}\}_3$ < $P\{C_6H_4\text{-}4\text{-}OMe\}_3$ for **2a**, **2b**, and **2c**. This trend parallels that associated with increase in electron donating ability of the phosphine.[33] The anomalous behavior of the mixed phosphine systems reveals, however, that care needs to be taken before drawing any more precise conclusions about how the electronic properties of the phosphine relate to these observations.

The relative enhancements of the hydride resonance of **2a** relative to those of **3a** and **3b**, and **2a** relative to those of **3a** and **3c** were also determined from these data. They proved to be 1:13.91:10.71 and 1:8:7.7, respectively. These data are not normalized since the ^{31}P signals for **3** could not be seen, but they clearly confirm that the family of *tris*-pyridine complexes **3** undergo significantly more rapid H_2 exchange than that of **2**. We have also examined analogous samples of **3a** and **3b**, and **3a** and **3c** at 330 K. The associated NMR spectra revealed that the relative signal enhancements for the hydride ligands of **3a/3b/3c** were 2.25:1:0.79. It therefore appears that **3a** undergoes more rapid exchange with H_2 than either **3b** or **3c**. In this case therefore the extent of enhancement follows the reduction in electron donating power of the phosphine.[33]

Table 2. Example Rate Constants for Equatorial Pyridine Ligand Exchange and Associated Activation Parameters for Exchange in Both **2** and **3**

complex	Rate (335 K)/s^{-1}	$\Delta H^{\ddagger}$/kJ mol^{-1}	$\Delta S^{\ddagger}$/J mol^{-1} K^{-1}	$\Delta G_{295}{}^{\ddagger}$/kJ mol^{-1}	$\Delta G_{335}{}^{\ddagger}$/kJ mol^{-1}
2a	0.40	134 ± 1	151 ± 5	89.1 ± 0.2	83.1 ± 0.02
2b	0.82	125 ± 3	132 ± 9	86.2 ± 0.3	81.0 ± 0.03
2c	0.90	155 ± 9	222 ± 28	89.7 ± 1	80.8 ± 0.14
3a	1.16	91 ± 8	34 ± 25	81.1 ± 1.0	79.7 ± 0.05
3b	2.00	107 ± 3	85 ± 8	81.9 ± 0.2	78.5 ± 0.08

We note that when EXSY spectroscopy was used to probe the hydride ligands in these complexes no exchange into free hydrogen was observed to occur in **2a** on the NMR time scale at 335 K. In contrast, around 4% of the hydride signal intensity transferred into that of H_2 when **3c** was examined at 335 K. It is therefore clear that the reductive elimination of H_2 from **2** or **3** under these conditions is not facile. Previous studies have suggested that H_2 elimination proceeds dominantly from 16-electron complexes such as $Ir(H)_2Cl(PPh_3)_2$ rather than 18-electron $Ir(H)_2Cl(PPh_3)_3$.[20] This process would therefore be expected to exhibit complex kinetic behavior, and given that its onset already pushes the temperature envelope of the solvent we have not explored it in more detail.[20]

Exchange of Bound and Free Pyridine Ligands by 2. EXSY spectroscopy was then employed to rigorously monitor the exchange rates of the bound pyridine ligand with free pyridine in **2** between 328 and 341 K. In all cases, the pyridine ligand that is *trans* to hydride was observed to undergo exchange with free pyridine.

For **2a**, the corresponding first order rate constant for pyridine dissociation proved to be 0.4 s^{-1} at 335 K, and values of $\Delta H^{\ddagger} = 134 \pm 1$ kJ mol^{-1} and $\Delta S^{\ddagger} = 151 \pm 5$ J mol^{-1} K^{-1} with $\Delta G_{295}{}^{\ddagger} = 89.1 \pm 0.2$ kJ mol^{-1} were determined for this process. For **2b** the corresponding rate constant proved to be 0.82 ± 0.008 s^{-1} at 335 K, and it can therefore be deduced that this process is faster in **2b** than **2a**. When this analysis method was repeated for **2c**, the corresponding rate constant at 335 K proved to be 0.90 s^{-1}. The associated activation parameters for this process are listed in Table 2.

The contributions of both the $\Delta S^{\ddagger}$ and the $\Delta H^{\ddagger}$ terms are largest for the most electron rich phosphine, $P\{C_6H_4\text{-}4\text{-}OMe\}_3$ of **2c**. However, their balance results in **2c** having the greatest pyridine exchange rate at 335 K. In the case of the related complex, $[Ir(NCMe)_2(PPh_3)_2(H)_2]^+$, the corresponding values are reported as 95.6 ± 2.3 kJ mol^{-1} and

(33) Tolman, C. A. *Chem. Rev.* **1977**, *77*, 313–348.

28.2 ± 7.1 J mol^{-1} K^{-1}, respectively.[34] The higher values of $\Delta H^{\ddagger}$ for pyridine loss in **2a**, than acetonitrile in $[Ir(NCMe)_2(PPh_3)_2(H)_2]^+$, agrees with the fact that the stronger pyridine donor should lead to the more costly rupture of a stronger Ir−N bond.

Exchange of Bound Pyridine and Free Pyridine in 3. A similar EXSY based procedure was used to study the exchange of pyridine in **3**. This process proved to be faster than that found for **2**. The associated rate constants and activation parameters for **3** are listed in Table 2. When **3a** was examined using this approach the dominant pathway again corresponded to exchange of the equatorial pyridine ligands with free pyridine. At the higher temperatures, however, there was evidence for the intercoversion of the axial and equatorial pyridine ligands within **3a**. At 340 K, and with a mixing time of 0.8 s, the proportion of pyridine loss was 60% while the level of axial−equatorial site exchange was only 4%. There were, however, no exchange peaks that connected the axial pyridine and free pyridine signals. These data therefore suggest that this process must occur via ligand interchange within the 16 electron intermediate $[Ir(PPh_3)(py)_2(H)_2]^+$ that is generated by pyridine loss *trans* to hydride in **3a** rather than by direct dissociation of the pyridine ligand which is *trans* to phosphine. These observations also require that in the 16-electron intermediate $[Ir(PPh_3)(py)_2(H)_2]^+$, the two pyridine ligands remain inequivalent, a situation that would certainly hold true in the solvent complex $[Ir(methanol)(PPh_3)(py)_2(H)_2]^+$ which might be expected in methanol. No such complications were evident in the case of **3b**, and the corresponding rates and activation parameters are listed in Table 2. In the case of **3b**, the corresponding rate constant for pyridine loss is 2.00 s^{-1} at 335 K and therefore a factor of 2.4 faster than that of **2b**. As a consequence the values of both $\Delta H^{\ddagger}$ and $\Delta S^{\ddagger}$ are reduced relative to those of **2**.

Much lower thermal stability was observed in the case of **3c** with decomposition occurring over time at temperatures above 308 K. We measured a rate for pyridine dissociation at this temperature of 0.066 s^{-1} but were unable to obtain activation parameters because of the decomposition. This situation was further complicated because weak exchange into a new species which was tentatively assigned to $[Ir(methanol)(P\{C_6H_4\text{-}4\text{-}OMe\}_3)(py)_2(H)_2]^+$ was observed. When the Eyring data are used to estimate the corresponding rate constants at 308 K for **3a** and **3b**, the values obtained are 0.068 ± 0.016 s^{-1} and 0.064 ± 0.004 s^{-1}, respectively. This confirms that at the lower temperatures, **3c** undergoes comparable exchange to **3a**, but clearly at the higher temperatures, where a large positive $\Delta S^{\ddagger}$ would work to enhance the difference, we cannot predict an order.

There is a significant difference in the relative magnitudes of the activation entropies for **3** when compared to **2**, and **3a** when compared to **3b**, even though they are essentially monitoring the same dissociation of pyridine. We note, however, that a higher level of associative character for the pyridine exchange step would lower $\Delta S^{\ddagger}$, as would increased ordering of the phosphine in the TS. Oro et al. have determined that the activation parameters for acetonitrile dissociation from the site *trans* to hydride in *fac-cis*-$[Ir(NCMe)_3(P^iPr_3)(H)_2]^+$ are $\Delta H^{\ddagger} = 112 \pm 4$ kJ mol^{-1} and $\Delta S^{\ddagger} = 135 = \pm 8$ J mol^{-1} K^{-1}.[27] The $\Delta S^{\ddagger}$ terms determined here for **3** are therefore not unusual.

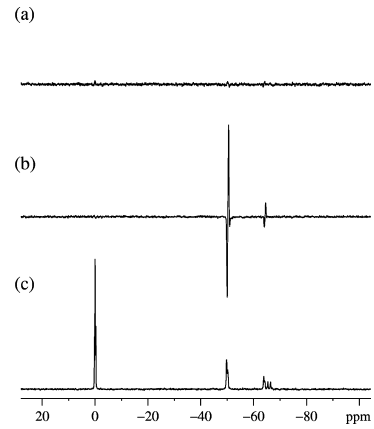

Figure 3. (a) 1024 scan ^{15}N control spectrum: (b) 16 scan ^{15}N detected PHIP-INEPT spectrum during the reaction of **1b** with parahydrogen in the presence of ^{15}N-labeled pyridine in methanol-d$_4$ (c) 64 scan ^{15}N detected PH-INEPT+EXSY spectrum of the same sample

In the case of the monophosphine systems **3a** and **3b**, both the values of $\Delta H^{\ddagger}$ are consistently smaller than those found for their *bis*-phosphine analogues. This suggests the Ir-py bond energy in **2** is higher than that in **3** thereby indicating that the second phosphine acts to strengthen the Ir−N bond when compared to pyridine. We note that while both pyridine and phosphine are σ-donors and π-acceptors, phosphine is the higher field ligand.

Magnetization Transfer from the PHIP Enhanced Hydride Signals to that of the ^{15}N Centre in Bound Pyridine. A series of heteronuclear polarization transfer experiments were then tested for their ability to transfer the hydride polarizations exhibited by **2** and **3** into the ^{15}N nuclei of the bound pyridine ligand. The NMR pulse sequences used were PH-INEPT, refocused PH-INEPT+, and PH-INEPT(+π/4) and have been reported previously.[25]

The associated NMR spectra were recorded for the same experimental setup and then the signal-to-noise ratios of the observed ^{15}N resonances measured and normalized according to the relative signal strengths of the hydride resonances seen in the corresponding ^{1}H NMR spectra that were recorded immediately before each ^{15}N magnetization transfer experiment. Without the *p*-H$_2$ based polarization transfer essentially no ^{15}N signals were visible after 1024 scans as shown in Figure 3a. The most efficient transfer of magnetization proved to be achieved using the PH-INEPT pulse sequence, and the corresponding 16 scan experiment is illustrated in Figure 3b. This situation arises because in the refocused version of this experiment, PH-INEPT+, relaxation during the refocusing period results in only a third of the potential signal intensity surviving to the point of observation. The

(34) Howarth, O. W.; McAteer, C. H.; Moore, P.; Morris, G. E. *Dalton Trans.* **1981**, 1481–1485.

Table 3. Comparison of ^{15}N Signal to Noise Ratios for the Indicated Heteronuclear Polarization Transfer Experiments Employing Complex **1a**

experiment	signal/noise[a]
PH-INEPT	27.9
PH-INEPT+	10.5
PH-INEPT(+π/4)	7.2

[a] Normalized using relative intensities of ^1H hydride signals recorded immediately before the polarization transfer experiments were conducted.

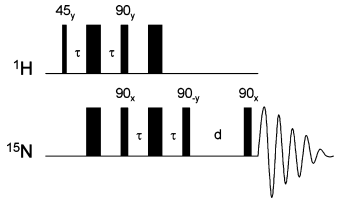

Figure 4. Schematic of the pulse sequence PH-INEPT+EXSY used for magnetization transfer where ($\tau = 1/4J_{HN}$).

PH-INEPT(+π/4) experiment was found to be least effective. These data are summarized in Table 3.

Magnetization Transfer from the PHIP Enhanced Hydride Signals to that of the ^{15}N Centre in Free Pyridine. Our main goal in these experiments was to transfer *p*-H_2 derived polarization from bound to free pyridine in a second step. This process would therefore lead to the polarization of a substrate that did not contain any protons that originated in the source of polarization, *p*-H_2. We therefore modified these polarization transfer experiments to store the ^{15}N magnetization in an I_z term prior to the introduction of a variable delay to facilitate magnetization transfer into the signal for free pyridine. This situation can be simply thought of as a heteronuclear EXSY experiment. The new pulse sequence, PH-INEPT+EXSY, is illustrated in Figure 4 where the polarization transfer sequence is followed by a $90°_{-y}$ storage pulse, and the magnetization transfer delay (*d*) is followed by a 90° observation pulse.

When this process was carried out on a sample containing enhanced proton signals for **2a** and **3a** it became clear that while polarization transfer to bound ^{15}N can be achieved, little or no exchange of magnetization corresponding to the ligated ligand exchanging into free pyridine occurs at 330 K. This is in direct agreement with the quantitative results described earlier.

The PH-INEPT+EXSY based data collection was then repeated on samples containing both **1b** and **1c**. The ^{15}N spectra now show significant signals for both bound pyridine and free pyridine. As the delay time used to encode ligand dissociation is increased from 0.1 to 1 s the proportion of signal that resides at the position of free pyridine clearly increases at the expense of the signals for the bound pyridine ligands of **3b**. These data are illustrated as a time course plot in Figure 5. A 64 scan spectrum with a reaction delay of 1 s is illustrated in Figure 3c for a system based on the precursor **1b**. The signal-to-noise ratio for the pyridine resonance in this 64 scan experiment is 198.4 and compares with the 1024 scan control experiments value of 6.64. This equates to a 120-fold increase in signal strength via polarization transfer.

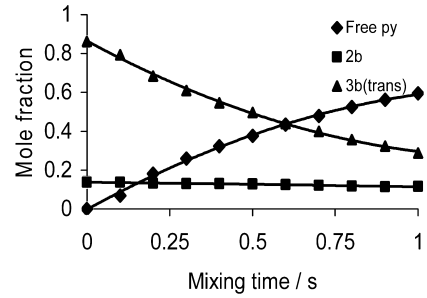

Figure 5. Plot of magnetization, as a mole fraction, for the equatorial pyridine signal sites, starting from **3b** versus reaction time obtained from PH-INEPT+EXSY data for a sample prepared from **1b**, ^{15}N-pyridine and *p*-H_2 at 330 K.

In the corresponding control experiments, using INEPT, and PH-INEPT sequences, no signal for free pyridine can be observed on this time scale. The control experiments therefore confirm that it is magnetization transfer from *p*-H_2 derived hyperpolarization sitting on the hydride ligands of **3b** that is responsible for these observations rather than magnetization transfer from the ring protons of free pyridine. These results represent the successful demonstration of the PHIP sensitization of an organic molecule that contains no nuclei that were previously located in parahydrogen.

Summary

In this paper we have demonstrated that $[Ir(PR_3)_2(py)_2(H)_2]BF_4$ and *fac*, *cis*-$[Ir(PR_3)(py)_3(H)_2]BF_4$ where R = Ph, *p*-tolyl and *p*-methoxyphenyl, undergo pyridine loss in a process that is influenced by the identity of the phosphine. The rate of pyridine ligand dissociation at 335 K proved to be highest for the most electron rich *p*-methoxyphenyl phosphine in the *bis*-pyridine complexes **2** which corresponds to the situation where both $\Delta H^{\ddagger}$ and $\Delta S^{\ddagger}$ are maximized. In contrast for **3**, the rate constants for pyridine loss in the *tris*-pyridine systems are all similar at 308 K, although they are larger than those determined for **2** (Table 2).

When these complexes are prepared using *p*-H_2 and ^{15}N-labeled pyridine was employed as the substrate, the parent complexes **2** and **3** show substantial PHIP enhancements in their hydride resonances. Magnetization transfer from the enhanced hydride signals of these species has been demonstrated to provide access to substantial ^{15}N signal enhancements in the bound pyridine ligand via the application of an INEPT based protocol. When such an approach is used in conjunction with a magnetization transfer step, the hyperpolarization that was originally based in *p*-H_2 is transferred first to a bound pyridine ligand in *fac*, *cis*-$[Ir(PR_3)(py)_3(H)_2]BF_4$ and then to free pyridine itself. This relayed magnetization transfer demonstrates that it is possible to employ the *p*-H_2 to sensitize the NMR signals of materials that have not been functionalized by an H_2 addition reaction. We have estimated that a 120-fold gain in the signal strength of the free pyridine resonances can be achieved via this route. It should be noted that since this means 1 scan equates to 14,400 scans without polarization there is therefore a significant reduction in the time necessary to record such information. Furthermore, since sensitivity relates to the square of the size of the magnetic

field, similar results could be achieved on a 103 T magnet which is around five times larger than that found in a 900 MHz system.

Previously, reactions with *p*-H_2 have been shown to enable the detection of metal dihydride complexes. It is not surprising, however, that when the protons that were previously located in *p*-H_2 are transferred into a hydrogen-acceptor such as an alkene, strong observable magnetization is also produced in the corresponding hydrogenation products. Recently this approach has been used to prepare hyperpolarized organic molecules for use as contrast agents in magnetic resonance imaging (MRI).[35] However, the need for the existence of a suitable hydrogen-acceptor reflects a significant limitation in the existing *p*-H_2 approach. The novelty of the procedure illustrated here is that it does not require the functionalization of a substrate through a formal hydrogenation step. Consequently it offers the opportunity to sensitize substrates where there is no dehydro-analogue available. We are continuing to explore the potential of this and other routes to sensitize the NMR experiment more generally.

Experimental Details

NMR measurements were made on Bruker DRX400 (^{1}H at 400.13 MHz, ^{31}P at 161 MHz, ^{15}N at 40 MHz), Bruker AV500 (^{1}H at 500.22 MHz, ^{31}P at 202.50 MHz, ^{15}N at 50.69 MHz), Bruker wide-bore AV600 (^{1}H at 600.12 MHz, ^{31}P at 242.93 MHz, ^{15}N at 60.81 MHz) and Bruker AV 700 (^{1}H at 700.12 MHz) NMR spectrometers. NMR samples were made up in 5 mm Young's tapped NMR tubes. Typical samples contained 1 mg of the iridium complex dissolved in CD_3OD (600 μL) with the other reagents being added by microsyringe. Samples were degassed at −78 °C and then pressurized with 3.5 bar *p*-H_2 before appropriate NMR measurements were recorded. *p*-H_2 was prepared by cooling the gas to 20 K over activated charcoal as described previously.[20]

X-ray data were obtained for a crystal of **2a** at 110 K using a Bruker Smart Apex diffractometer with Mo Kα radiation (ν = 0.71073 Å) in conjunction with a SMART CCD camera. Diffractometer control, data collection, and initial unit cell determination were performed using "SMART" (v5.625 Bruker-AXS). Frame integration and unit-cell refinement were carried out with the "SAINT+" (v6.22, Bruker AXS) package. Absorption corrections were applied by SADABS (v2.03, Sheldrick). The structure was solved by Patterson map using ShelXS (Sheldrick, 1997) and refined using ShelXL (Sheldrick, 1997). Crystals were grown from a benzene solution of **1a** which contained H_2 and pyridine.

Syntheses. All reactions were carried out under N_2 using glovebox or Schlenk line techniques. Dichloromethane and diethyl ether were distilled over calcium hydride and sodium benzophenyl ketyl, respectively, prior to use. Tri(phenyl)phosphine (Aldrich), tri(*p*-tolyl)phosphine (Strem), tri(anisolyl)phosphine (Strem), pyridine (Aldrich), and ^{15}N-pyridine (Cambridge Isotopes) were used as supplied and stored under N_2. $[Ir(COD)(PPh_3)_2]BF_4$ (**1a**) and $[Ir(COD)(NCMe)_2]BF_4$ were prepared by literature methods.[26,29,36,37]

$[Ir(COD)(P\{p\text{-}tolyl\}_3)_2]BF_4$ (1b). The known complex **1b** was prepared as follows: $[Ir(COD)(NCMe)_2]BF_4$ (150 mg, 0.32 mmol) was dissolved in dichloromethane (5 mL) to which was added by canula P(*p*-tolyl)$_3$ (195 mg, 0.64 mmol) in dichloromethane (5 mL). After stirring for 15 min, the volume was reduced in vacuo and diethyl ether added to precipitate the product. The dark pink/red solid was then washed with diethyl ether (5 mL) and dried under vacuum. Yield: 197 mg (62%): ^{31}P NMR: δ 16.1.

$[Ir(COD)(P\{C_6H_4\text{-}4\text{-}OMe\}_3)_2]BF_4$ (1c). The known complex **1c** was prepared as follows: A Schlenk tube was charged with $[Ir(COD)Cl]_2$ (250 mg, 0.37 mol) and $AgBF_4$ (160 mg, 0.82 mmol). To this was added a degassed methanol (10 mL) solution of P(C_6H_4-4-OMe)$_3$ (521 mg, 1.48 mmol), and the resulting suspension stirred overnight in the absence of light. The solvent was then completely removed under vacuum, and the product extracted into CH_2Cl_2 (10 mL). The suspension was filtered through celite, and the red filtrate concentrated to about 1 mL before Et_2O (10 mL) was added to precipitate the product. After washing with Et_2O (3 × 2 mL) and drying in vacuo for 1 h a dark red powder was obtained. Yield: 640 mg, 79%. ^{31}P NMR: δ 14.9

Exchange of IrH for IrD. It should be noted that during the course of all of these reactions in CD_3OD, the slow exchange of a deuterium label into the hydride sites of **2** and **3** was observed. After 24 h, the corresponding hydride resonances were very weak, or no longer visible, because of total exchange to the corresponding deuterides. Both CD_3OH and HD signals were also visible in these spectra.

Selected NMR data for $[Ir(py)_2(PPh_3)(P\{p\text{-}tolyl\}_3)(H)_2]BF_4$. ^{1}H: Hydride: δ −21.72, (J_{PH} = 19 Hz, J_{NH} = 23 Hz); ^{31}P: PPh_3 δ 23.17 (d J_{PP} = 344 Hz), P{*p*-tolyl}$_3$, δ 20.47 (d, J_{PP} = 344 Hz), ^{15}N: δ −63.3.

Selected NMR data for $[Ir(py)_2(PPh_3)(P\{C_6H_4\text{-}4\text{-}OMe\}_3)(H)_2]BF_4$. ^{1}H: Hydride: δ −21.72, (J_{PH} = 21 Hz, J_{NH} = 21 Hz); ^{31}P: PPh_3 δ 22.86 (d J_{PP} = 348 Hz), P{C_6H_4-4-OMe}$_3$, δ 18.35 (d, J_{PP} = 348 Hz), ^{15}N: δ −61.1.

Acknowledgment. We wish to thank the University of York and a White Rose initiative for part funding this work through its technology transfer scheme. Other financial support from the Spanish MEC (Project Consolider ORFEO (CSD 2007-00006)) and the MRC (K.D.A.) are also acknowledged. We are also grateful to Bruker BioSpin and Mark Mortimer for particularly helpful discussions.

Supporting Information Available: Tables containing rates and activation parameters for pyridine exchange and X-ray information for **2a** (CCDC 699760). This material is available free of charge via the Internet at http://pubs.acs.org.

IC8020029

(35) Goldman, M.; Johannesson, H.; Axelsson, O.; Karlsson, M. *C. R. Chim.* **2006**, *9*, 357–363.

(36) Crabtree, R. H.; Mellea, M. F.; Mihelcic, J. M.; Sen, A.; Chebolu, V. *Inorg. Synth.* **1989**, *26*, 122–126.

(37) Crabtree, R. H.; Hlatky, G. G.; Parnell, C. P.; Segmuller, B. E.; Uriarte, R. J. *Inorg. Chem.* **1984**, *23*, 354–358.